Journal of Solid Mechanics Vol. 10, No. 4 (2018) pp. 816-830

Investigation of Pre-buckling Stress Effect on Buckling Load Determination of Finite Rectangular Plates with Circular Cutout

S. Abolghasemi[1,*], H.R. Eipakchi[1], M. Shariati[2]

[1]*Faculty of Mechanical and Mechatronic Engineering, Shahrood University of Technology, Shahrood, Iran*
[2]*Department of Mechanical Engineering, Ferdowsi University of Mashhad, Mashhad, Iran*

Received 23 July 2018; accepted 26 September 2018

ABSTRACT

This paper investigates the buckling of finite isotropic rectangular plates with circular cutout under uniaxial and biaxial loading. The complex potential method is used to calculate the pre-buckling stress distribution around the cutout in the plate with finite dimensions. To satisfy the in-plane boundary conditions, the generalized complex-potential functions are introduced and a new method based on the boundary integral which has been obtained from the principle of virtual work is used to apply the boundary conditions at the plate edges. The potential energy of the plate is calculated by considering the first order shear deformation theory and the Ritz method is used to calculate the buckling load. The effects of cutout size, type of loading and different boundary conditions on the buckling load are investigated. Comparing of the calculated buckling loads with the finite element results shows the accuracy of the presented method for buckling analysis of the plates.

Keywords: Circular cutout; Complex potential functions; Ritz method; Buckling; Finite rectangular plate; Shear deformation.

1 INTRODUCTION

PLATES are initially flat structures which are extensively used in many fields of engineering such as architectural structures, airplanes, ships, etc. In some applications, cutouts with different shapes are introduced in the plates to provide access for inspection, services, maintenance, ventilation or decreasing the weight. The existence of cutout alters the stress distribution in the plate and consequently influences its buckling behavior. One approach to calculate the stress distribution around a hole in an infinite plate is the complex potential method. This method was introduced by Lekhnitskii [1] and Savin [2] to calculate the stress concentration factor around a circular hole in an infinite orthotropic plate. Savin used the Schwarz–Christoffel integral mapping for calculating the potential functions, while Lekhnitskii used the Fourier series, however their solutions were the same. A review of the mathematical basis of the complex potential method and the related studies was presented by Sevenois and Koussios [3]. An analytical solution was presented by Lin and Ko [4] for determining the stress concentration factor of finite composite laminates with an elliptical cutout. The solution was obtained by the complex variable technique in conjunction with the boundary collocation method. Gao [5] presented a general solution for calculating the stress

*Corresponding author. Tel.: +98 23 32300258; Fax: +98 23 9127730968.
E-mail address: saeedabolghasemi2003@yahoo.com (S.Abolghasemi).

distribution in an infinite elastic plate with an elliptical hole and subjected to arbitrary biaxial loading. He used the complex potential method in the elliptic-hyperbolic coordinate system to obtain the solution. Ukadgaonker and Rao [6] used Savin's formulation and a superposition method to present a solution for stress distribution around an arbitrarily shaped hole in symmetric laminates subjected to any combination of in-plane loads. Xu and Yue [7] studied the stress distribution in finite composite laminates with multiple cutouts. They employed the complex potential method based on the series expansion and least squares boundary collocation method. Louhghalam et al. [8] used a combined conformal mapping and Finite Element (FE) approach to calculate the stress concentration factor in a plate with multiple rectangular cutouts under bending deformation. Nemeth et al. [9] used an approximate method for buckling analysis of rectangular composite plates with a circular cutout. By expressing the displacements as the product of two series of functions, they were able to convert the pre-buckling and buckling problems from two-dimensional case to a one-dimensional system of linear differential equations with variable coefficients, which were solved by the finite difference method. Britt [10] studied the buckling of biaxial and shear loaded anisotropic panels with an elliptical cutout. He used the complex potentials and a boundary collocation method to calculate the pre-buckling stress distribution. Buckling analysis of plates with eccentrically located rectangular cutouts was performed by Shakerley and Brown [11]. They used the conjugate load-displacement method to calculate the buckling loads. In many studies related to the buckling of plates with cutout, the solution is based on the FE or other numerical methods [12-21], since the existence of cutout complicates the pre-buckling stress distribution in the plate. El-sawy and Nazmy [12] used the FE method to study the buckling of rectangular plates with circular and rectangular cutouts located at different locations in the plate. Ghannadpour et al. [14] performed a study on the buckling of rectangular composite plates with cutout by using the FE method. Also Anil et al. [15] used the FE formulation based on the higher order shear deformation theory to study the buckling of composite laminates with rectangular cutout under biaxial loading. The effect of single and multiple holes on the buckling of plates was demonstrated by Moen and Schafer [16]. They presented closed-form expressions by a numerical analysis for approximating the critical stresses. Kumar and Sing [17-19] studied the stability and failure of composite plates with cutouts of various shapes, such as square, circle, diamond and ellipse by the FE method. Prajapat et al. [21] investigated the buckling of perfect and perforated plates subjected to four different in-plane boundary conditions. Barut and Madenci [22] used a complex potential-variational formulation to study the thermo-mechanical buckling of flat laminates with an elliptical cutout at an arbitrary location and orientation. Ovesy and Fazilati [23] used the third order shear deformation theory to calculate the buckling load and natural frequency of composite plates with circular and square cutouts using the finite strip method. Huang and Leissa [24] used the Ritz method with special displacement functions to study the vibrations of rectangular plates with side cracks of different size, location and orientation. Also Huang et al. [25] used a new set of admissible functions in the Ritz method to properly describe the stress singularity near the tips of crack and used this method to study the vibrations of simply supported and free square plates with internal cracks based on the classical plate theory (*CPT*) without in-plane loading. It is noted that in the study of free vibration in presence of the in-plane load, there is no need to calculate the pre-buckling stress field, which is a major step in the buckling analysis of the plates with cutout.

In this paper, the complex potential method has been used to calculate the pre-buckling stress distribution in a finite plate with circular cutout. This solution satisfies the boundary conditions at the cutout edge exactly. The potential energy of the plate is extracted based on the first order shear deformation theory (*FSDT*) and the Ritz method is used to calculate the buckling load. By using the analytical solution, some new results are presented for the buckling load of a plate with circular cutout and different boundary conditions under uniaxial and biaxial loading. In summary:

- Instead of collocation method, which has difficulties regarding to point spacing and the number of required points for a good accuracy, a boundary integral which is obtained from the principle of virtual work is employed to apply the in-plane boundary conditions at the plate edges. This method satisfies the boundary conditions at the cutout edge exactly and the boundary condition at plate edges with high accuracy.
- The vibration mode shapes of a beam with the same boundary conditions of the plate are used as trial functions in the Ritz method to calculate the buckling load of a plate with cutout. To the knowledge of the authors, this method has not been applied to plates with cutout.

2 PROBLEM FORMULATION

2.1 Pre-buckling stress distribution

The method of complex potentials is used to calculate the pre-buckling stress field of a plate with circular cutout. The compatibility equation for a two-dimensional problem is:

$$\nabla^4\phi = \frac{\partial^4\phi}{\partial x^4} + 2\frac{\partial^4\phi}{\partial x^2 \partial y^2} + \frac{\partial^4\phi}{\partial y^4} = 0 \tag{1}$$

and the solution is expressed as: [26]

$$\phi(z,\bar{z}) = 1/2(z\,\overline{\gamma(z)} + \bar{z}\,\gamma(z) + \chi(z) + \overline{\chi(z)}) = \mathrm{Re}(\bar{z}\,\gamma(z) + \chi(z)) \tag{2}$$

where $z = x + iy$ is the complex variable and $\gamma(z), \chi(z)$ are arbitrary functions of z.

Now by defining $\psi(z) = \chi'(z)$, the stress components are calculated as the following:

$$\sigma_x = 2\,\mathrm{Re}[\gamma'(z) - \frac{1}{2}\bar{z}\,\gamma''(z) - \frac{1}{2}\psi'(z)],\ \sigma_y = 2\,\mathrm{Re}[\gamma'(z) + \frac{1}{2}\bar{z}\,\gamma''(z) + \frac{1}{2}\psi'(z)],\ \tau_{xy} = \mathrm{Im}[\bar{z}\,\gamma''(z) + \psi'(z)] \tag{3}$$

The boundary condition is expressed as:

$$T_x + iT_y = -i\frac{d}{ds}(\frac{\partial\phi}{\partial x} + i\frac{\partial\phi}{\partial y}) = -i\frac{d}{ds}(\frac{\partial\phi}{\partial\bar{z}}) = -i\frac{d}{ds}(\gamma(z) + z\,\overline{\gamma'(z)} + \overline{\psi(z)}) \tag{4}$$

where T_x, T_y are traction force vectors applied at the boundaries of the plate (Fig. 1). By integrating Eq. (4) results:

$$F_x + iF_y = \int_A^B (T_x + iT_y)ds = -i\int_A^B \frac{d}{ds}(\gamma(z) + z\,\overline{\gamma'(z)} + \overline{\psi(z)})ds = -i\,[\gamma(z) + z\,\overline{\gamma'(z)} + \overline{\psi(z)}]_A^B \tag{5}$$

where F_x, F_y are resultant force components acting on a segment of the boundary from *A* to *B* (Fig. 1).

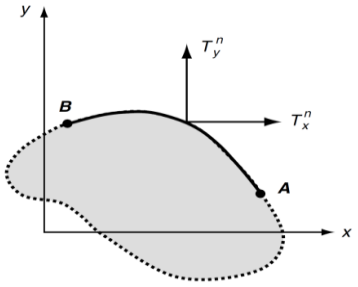

Fig.1
Traction force vectors applied at plate boundaries.

The problem solution now reduces to finding two complex potential functions $\gamma(z)$ and $\psi(z)$ that satisfy the boundary condition as stated in Eq. (5). Then, the in-plane stress components are calculated from Eqs. (3). In this paper, the complex functions $\gamma(z)$ and $\psi(z)$ for finite plates are expressed as:

$$\gamma(z) = \sum_{n=1}^{N_1} A_n z^n + \sum_{n=1}^{N_2} \frac{B_n}{z^n},\quad \psi(z) = \sum_{n=1}^{N_1} C_n z^n + \sum_{n=1}^{N_2} \frac{D_n}{z^n} \tag{6}$$

where N_1 and N_2 are the number of terms considered for each series.

2.2 In-plane boundary conditions

The constants A_n, B_n, C_n and D_n in Eq. (6) must be calculated from the in-plane boundary conditions. In this paper, the boundary conditions are applied in two steps. At first, Eq. (5) is used to apply the boundary condition at

the cutout edge. By solving the obtained system of equations, in which the number of equations is less than the number of unknowns, some of these constants are calculated. Then, based on the principle of virtual work, a boundary integral is obtained that is used to apply the boundary conditions at the plate edges and to calculate the remaining constants. This method is explained in the following. The displacement field of a plate subjected to in-plane loading without the lateral deflection is expressed as:

$$u = u_0(x, y),\ v = v_0(x, y),\ \mathrm{w} = 0 \tag{7}$$

According to the principle of virtual work, in an equilibrium state the relation $\delta W_I + \delta W_E = 0$ holds, where δW_I and δW_E are the virtual work of internal and external forces, respectively, which are expressed as: [27]

$$\begin{aligned} \delta W_I &= \iiint_V (\sigma_x \delta\varepsilon_x + \sigma_y \delta\varepsilon_y + \sigma_z \delta\varepsilon_z + \tau_{xy} \delta\gamma_{xy} + \tau_{xz} \delta\gamma_{xz} + \tau_{yz} \delta\gamma_{yz}) dV \\ \delta W_E &= \int_C \left(N_x^0 \delta u_0 dy + N_y^0 \delta v_0 dx + N_{xy}^0 \left(\delta v_0 dy - \delta u_0 dx \right) \right) \end{aligned} \tag{8}$$

where N_x^0, N_y^0 and N_{xy}^0 are the stress resultants applied at the plate edges. By substituting the strain components in the virtual work relation and using the Green's theorem, we have

$$\begin{aligned} \delta W_I + \delta W_E &= \iint_A \left(\left(-\frac{\partial N_x}{\partial x} - \frac{\partial N_{xy}}{\partial y} \right) \delta u_0 + \left(-\frac{\partial N_y}{\partial y} - \frac{\partial N_{xy}}{\partial x} \right) \delta v_0 \right) dA \\ &+ \int_C \left(\left(N_x dy - N_{xy} dx + N_x^0 dy - N_{xy}^0 dx \right) \delta u_0 + \left(N_{xy} dy - N_y dx + N_y^0 dx + N_{xy}^0 dy \right) \delta v_0 \right) = 0 \end{aligned} \tag{9}$$

where N_x, N_y, N_{xy} are stress resultants which are expressed as:

$$\left\{ N_x, N_y, N_{xy} \right\} = \int_{-h/2}^{h/2} \left\{ \sigma_x, \sigma_y, \tau_{xy} \right\} dz \tag{10}$$

where h is thickness of the plate. Eq. (9) contains two integrals, one in the domain of problem and the other over the boundary. For the virtual work principle to be held, the coefficients of δu_0 and δv_0 in each integral must be equated to zero, which give the equilibrium equations and boundary conditions of the problem. The equilibrium equations were solved by using the complex potentials in the previous section. Now the second integral in Eq. (9) is used to apply the boundary conditions at the plate outer edges. To do this, the displacement components u_0 and v_0 must be known. The equilibrium equations in terms of the displacements, referred to Navier's equations are expressed as: [26]

$$G\nabla^2 \mathbf{u} + (\lambda + G)\nabla(\nabla . \mathbf{u}) = 0 \tag{11}$$

where $\nabla = \frac{\partial}{\partial x} \hat{i} + \frac{\partial}{\partial y} \hat{j}$ is the gradient operator and $\mathbf{u} = \{u_0, v_0\}^T$ is the displacement vector. By introducing the complex displacement $U = u + iv$ in the Navier's equation, it is written in the complex form as:

$$(\lambda + G) \frac{\partial}{\partial \bar{z}} \left(\frac{\partial U}{\partial z} + \frac{\partial \bar{U}}{\partial z} \right) + 2G \frac{\partial^2 U}{\partial \bar{z} \partial z} = 0 \tag{12}$$

By integrating the above equation, the complex displacement U is calculated as a function of complex potentials as follows:

$$2GU = \kappa \gamma(z) - z\,\overline{\gamma'(z)} + \overline{\psi(z)} \tag{13}$$

where $\kappa=(3-\nu)/(1+\nu)$ for the plane stress conditions. After solving Eq. (13) for u_0 and v_0, the variations δu_0 and δv_0 are calculated. Now to apply the boundary conditions at the plate edges, the values of resultant forces N_x, N_y and N_{xy} and also the variations δu_0 and δv_0 are substituted in the boundary integral (the second integral in Eq. (9)). By equating the coefficients of $\delta A_i, \delta B_i, \delta C_i$ and δD_i to zero in the obtained expression, the unknown constants are calculated. After calculation of the constants in Eq. (6), the pre-buckling stress distribution is obtained by substituting $\gamma(z)$ and $\psi(z)$ into Eqs. (3). In the next step, this stress distribution is used to calculate the buckling load. Since the expressions obtained for pre-buckling stress components are very complicated, direct solution of the stability equations is difficult. In this paper, the potential energy of the plate is calculated based on the first order shear deformation theory and the Ritz method is used to calculate the buckling load.

2.3 Energy of plate based on FSDT

Consider an isotropic and homogeneous plate with length *a*, width *b* and thickness *h*. A coordinate system which its origin is located at the plate center and *x,y,z* axes are along the plate length, width and thickness, respectively, is used to describe the displacements (Fig. 2). The displacement field of a deformed plate according to FSDT is expressed as: [27]

$$u=u_0(x,y)+zu_1(x,y), v=v_0(x,y)+zv_1(x,y), w=w(x,y). \tag{14}$$

where u_0, v_0, w represent the displacement components of a point on the mid-plane (z=0) and u_1, v_1 represent the rotation of a line initially perpendicular to the mid-plane relative to y and x axes, respectively. The total potential energy of the plate during lateral deflection is $\Pi=V_1+V_2$ where V_1 is the strain energy and V_2 is the potential energy due to in-plane loads during lateral deflection. These energies are expressed as: [28]

$$\begin{aligned} V_1&=\frac{1}{2}\iint_S\left(\{M_x,M_y,M_{xy}\}\left\{\frac{\partial u_1}{\partial x},\frac{\partial v_1}{\partial y},\frac{\partial u_1}{\partial y}+\frac{\partial v_1}{\partial x}\right\}^T+\{Q_x,Q_y\}\left\{u_1+\frac{\partial w}{\partial x},v_1+\frac{\partial w}{\partial y}\right\}^T\right)dS,\\ V_2&=\frac{1}{2}\iint_S\left(N_x\left(\frac{\partial w}{\partial x}\right)^2+N_y\left(\frac{\partial w}{\partial y}\right)^2+2N_{xy}\frac{\partial w}{\partial x}\frac{\partial w}{\partial y}\right)dS. \end{aligned} \tag{15}$$

where *S* is the mid-plane area. The moment and transverse shear resultants are:

$$\begin{Bmatrix}M_x\\M_y\\M_{xy}\end{Bmatrix}=\int_{-h/2}^{h/2}\begin{Bmatrix}\sigma_x\\\sigma_y\\\tau_{xy}\end{Bmatrix}z\,dz,\quad \begin{Bmatrix}Q_x\\Q_y\end{Bmatrix}=k_s\int_{-h/2}^{h/2}\begin{Bmatrix}\tau_{xz}\\\tau_{yz}\end{Bmatrix}dz \tag{16}$$

where k_s =5/6 is the shear correction factor [27]. The moment and transverse shear resultants are related to displacements as the following:

$$\begin{Bmatrix}M_x\\M_y\\M_{xy}\end{Bmatrix}=\frac{h^3}{12}\begin{bmatrix}A&\lambda&0\\\lambda&A&0\\0&0&G\end{bmatrix}\begin{Bmatrix}\frac{\partial u_1}{\partial x}\\\frac{\partial v_1}{\partial y}\\\frac{\partial u_1}{\partial y}+\frac{\partial v_1}{\partial x}\end{Bmatrix},\quad \begin{Bmatrix}Q_x\\Q_y\end{Bmatrix}=k_sGh\begin{bmatrix}1&0\\0&1\end{bmatrix}\begin{Bmatrix}u_1+\frac{\partial w}{\partial x}\\v_1+\frac{\partial w}{\partial y}\end{Bmatrix}. \tag{17}$$

where $A=\lambda+2G$ and G,λ are Lame's constants which are expressed as:

$$\lambda = \frac{E\nu}{(1+\nu)(1-2\nu)},\ G = \frac{E}{2(1+\nu)}. \tag{18}$$

By substituting Eqs. (16) and (10) into Eq. (15), the total potential energy can be written as a function of pre-buckling stress components and displacement field u_1, v_1, w . In the Ritz method, the potential energy of the plate is approximated by assuming appropriate functions for displacements. Here the displacements are expressed as:

$$\mathrm{u}_1(x,y) = \sum_{m=1}^{M}\sum_{n=1}^{N} U_{m,n}\phi_{1m}(x)\psi_{1n}(y),\ v_1(x,y) = \sum_{m=1}^{M}\sum_{n=1}^{N} V_{m,n}\phi_{2m}(x)\psi_{2n}(y),\ w(x,y) = \sum_{m=1}^{M}\sum_{n=1}^{N} W_{m,n}\phi_{3m}(x)\psi_{3n}(y) \tag{19}$$

where ϕ_{im} , ψ_{in} , $i = 1,2,3$ are admissible functions that satisfy the essential boundary conditions of the problem.

Kumar presented a complete review on the application of the Ritz method for vibration and buckling analysis of plates and shells [29]. There are different sets of admissible functions that can be used in the Ritz method. Garcia et al. [30] compared the accuracy, convergence and numerical behavior of different sets of admissible functions in the Ritz method. In this paper, the lateral vibrational mode shapes of a beam with boundary conditions similar to the plate in two opposite edges has been used to express $\phi_m(x)$ and $\psi_n(y)$. These functions have the property of completeness and orthogonality which improves the convergence of the solution. The differential equation for free vibration of an Euler-Bernoulli beam with density ρ , Young's modulus *E*, cross sectional area A_0 and moment of inertia *I* is expressed as:

$$EI\frac{\partial^4 w(x,t)}{\partial x^4} + \rho A_0 \frac{\partial^2 w(x,t)}{\partial t^2} = 0 \tag{20}$$

where $w(x,t)$ is deflection of the beam.

The solution of Eq. (20) is considered as $w(x,\mathrm{t}) = \phi(x)\cos(\omega \mathrm{t})$ where $\phi(x)$ represents the vibrational mode shape of the beam. The solution is expressed as $\phi(x) = C_1\cos(\beta \mathrm{x}) + C_2\sin(\beta x) + C_3\cosh(\beta x) + C_4\sinh(\beta \mathrm{x})$ where $\beta^4 = \frac{\rho A_0}{EI}\omega^2$. Now by applying the boundary conditions at two ends of the beam, the vibrational mode shapes and the value of β are calculated. The beam functions for different combinations of boundary conditions are as follows:

a) simply supported at both ends

$$\phi_m^{ss}(x) = \sin(\beta_m \mathrm{x}),\ \beta_m = \frac{m\pi}{a},\ (m = 1,2,...)$$

where *a* is the length of the beam.

b) clamped at both ends

$$\phi_m^{cc}(x) = \frac{\cos(\beta_m \mathrm{a}) - \cosh(\beta_m \mathrm{a})}{\sin(\beta_m \mathrm{a}) - \sinh(\beta_m \mathrm{a})}\left(\sin(\beta_m x) - \sinh(\beta_m \mathrm{x})\right) + \cosh(\beta_m \mathrm{x}) - \cos(\beta_m \mathrm{x}),\ (m = 1,2,...)$$

where β_m is the solution of $\cos(\beta_m \mathrm{a})\cosh(\beta_m \mathrm{a}) - 1 = 0$.

c) simply supported at left end and free at right end

$$\phi_1^{sf}(x) = x,\ \phi_m^{sf}(x) = \frac{\sinh(\beta_m \mathrm{a})}{\sin(\beta_m \mathrm{a})}\sin(\beta_m \mathrm{x}) + \sinh(\beta_m \mathrm{x}),\ (m = 2,3,...)$$

where $\beta_1 = 0$ and $\beta_m, \mathrm{m} = 2,3,...$ is the solution of $\tan(\beta_m\ \mathrm{a}) - \tanh(\beta_m\ \mathrm{a}) = 0$

d) free at both ends

$$\phi_1^{ff}(x) = 1,\ \phi_2^{ff}(x) = x,\ \phi_m^{ff}(x) = \frac{\cos(\beta_m\ \mathrm{a}) - \cosh(\beta_m\ \mathrm{a})}{\sin(\beta_m\ \mathrm{a}) - \sinh(\beta_m\ \mathrm{a})}\left(\sin(\beta_m x) + \cosh(\beta_m\ \mathrm{x})\right) + \cos(\beta_m\ \mathrm{x}) + \sinh(\beta_m\ \mathrm{x}),\ (m = 3,4,...)$$

where $\beta_1 = \beta_2 = 0$ and $\beta_m, m = 3,4,...$ is the solution of $\cos(\beta_m\ \mathrm{a})\cosh(\beta_m\ \mathrm{a}) - 1 = 0$.

The functions $\psi_n(y)$ are constructed by replacing *x, a* and *m* by *y, b* and *n,* respectively, in the corresponding $\phi_m(x)$ function. For example, for a simply supported plate at the left and right edges and clamped at the up and down edges, the displacement field is expressed as:

$$\mathrm{u}_1(x,y) = \sum_{m=1}^{M}\sum_{n=1}^{N} U_{m,n}\phi_m'^{ss}(x)\psi_n^{cc}(y),\ v_1(x,y) = \sum_{m=1}^{M}\sum_{n=1}^{N} V_{m,n}\phi_m^{ss}(x)\psi_n'^{cc}(y),\ w(x,y) = \sum_{m=1}^{M}\sum_{n=1}^{N} W_{m,n}\phi_m^{ss}(x)\psi_n^{cc}(y)$$

At an equilibrium state, the total potential energy of the system is stationary , i.e

$$\delta\Pi = \sum_{m=1}^{M}\sum_{n=1}^{N}\left(\frac{\partial\Pi}{\partial U_{m,n}}\delta U_{m,n} + \frac{\partial\Pi}{\partial V_{m,n}}\delta V_{m,n} + \frac{\partial\Pi}{\partial W_{m,n}}\delta W_{m,n}\right) = 0 \Rightarrow \frac{\partial\Pi}{\partial U_{m,n}} = 0,\ \frac{\partial\Pi}{\partial V_{m,n}} = 0,\ \frac{\partial\Pi}{\partial W_{m,n}} = 0 \qquad (21)$$

By substituting the expression for total potential energy into Eqs. (21), an eigenvalue problem is obtained and the buckling loads and mode shapes are calculated.

3 FE ANALYSIS

In order to evaluate the accuracy of the presented solution, the FE analysis has been performed by using ABAQUS package. The S4R element has been used for meshing. This element is a 4-node quadrilateral shell element with reduced integration and a large-strain formulation, which is suitable for analyzing thick or thin plates and shells [31].The size of elements has been selected based on a mesh sensitivity analysis. The in-plane loads are applied as "shell edge load" type at corresponding edges.

4 RESULTS AND DISCUSSION

4.1 Pre-buckling

In this section, the pre-buckling stress distribution for an isotropic square plate with a circular cutout and subjected to in-plane loading is presented. The geometry of the plate is shown in Fig. 2, where $\lambda = 0$ represents uniaxial loading and $\lambda = 1$ represents biaxial loading.

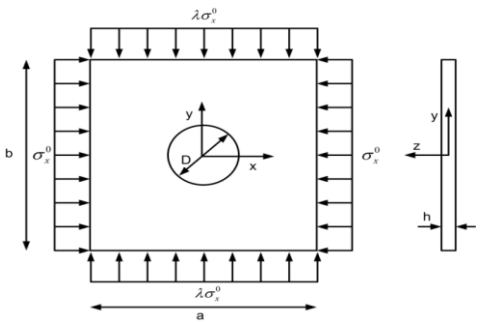

Fig.2
Geometry of plate with cutout under in-plane loading.

In Fig. 3, the variation of tangential stress σ_θ around the circular hole has been shown for different values of D/a. For an infinite plate, the value of stress concentration factor $(\sigma_\theta^{\max}/\sigma_x^0)$ is equal to 3 for uniaxial and 2 for biaxial loadings [26], where $\sigma_\theta^{\max}, \sigma_x^0$ are the maximum stress around the cutout and the in-plane stress applied at the plate edges, respectively. Fig. 3 shows that for finite plates, the stress concentration factor is higher than infinite plate and its value increases as the D/a ratio increases. The variation of tangential stress around the cutout is different for uniaxial and biaxial loading. In the case of biaxial loading, the tangential stress is almost constant around the cutout for small holes (smaller values of D/a ratios), but as the hole size increases, tangential stress changes with θ and the maximum stress occurs at 45° (on diagonal lines) and repeats at 90° intervals. For uniaxial loading, the maximum stress occurs at 90° and repeats at 180° intervals.

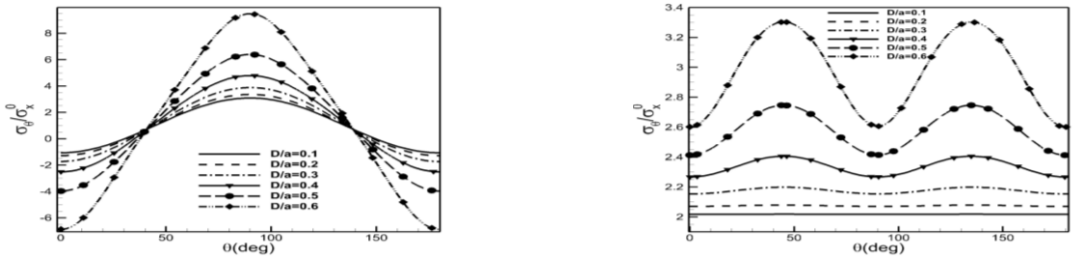

(a) (b)

Fig.3
Variation of tangential stress around circular cutout. a) uniaxial loading. b) baxial loading.

The variation of in-plane stress components at different cross sections for a plate with $D/a = 0.6$ under uniaxial loading has been shown in Fig. 4, where R is the cutout radius. In equilibrium state, the area under each curve in σ_x/σ_x^0 graphs must be equal to one and the area under each curve in σ_y/σ_x^0 and τ_{xy}/σ_x^0 graphs must be equal to zero for this case, and the calculations show this fact. In order to investigate the accuracy of the presented solution in satisfying the boundary conditions at the plate edges, the variation of in-plane stress components along plate edges has been shown in Fig. 5 for a plate under uniaxial loading with $D/a = 0.6$. According to this Figure, the maximum error in satisfying the boundary conditions at the plate edges is less that 1.5%. This error has been defined as: error (%)= (actual value-calculated value)/actual value*100. It has smaller values for lower value D/a.

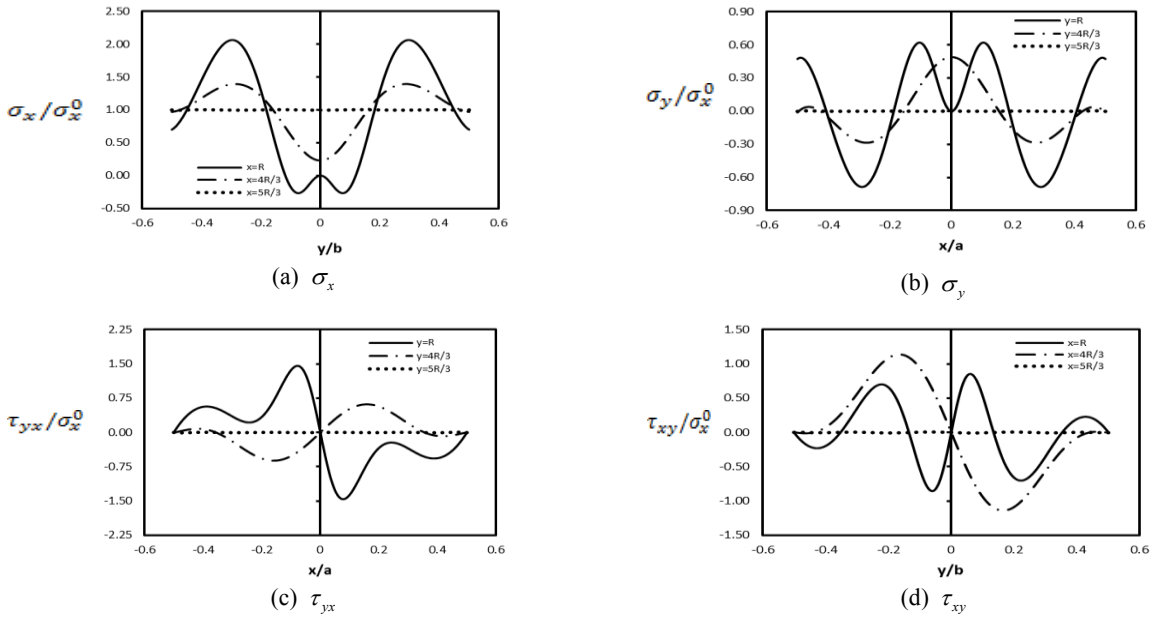

(a) σ_x (b) σ_y

(c) τ_{yx} (d) τ_{xy}

Fig.4
Variation of in-plane stress components for a plate under uniaxial loading with $D/a = 0.6$.

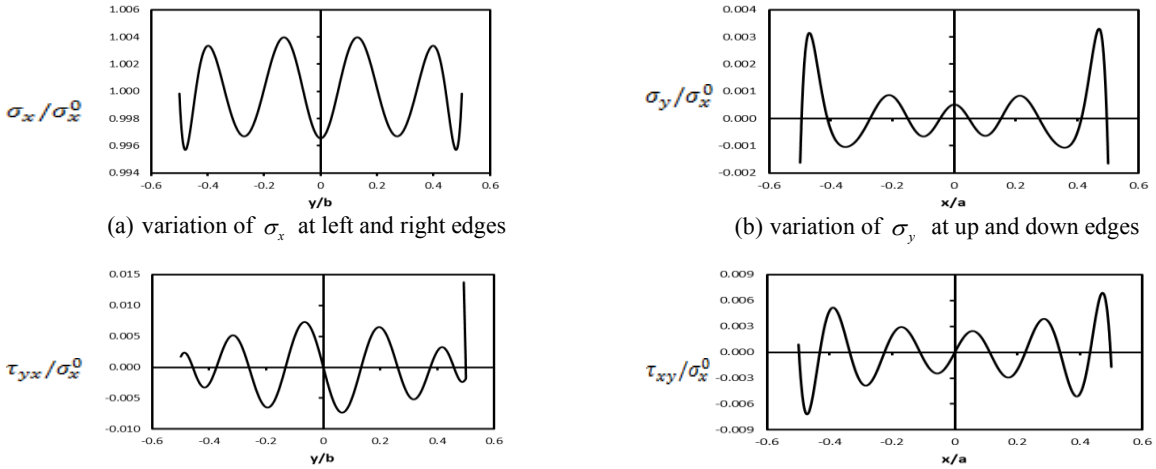

(a) variation of σ_x at left and right edges

(b) variation of σ_y at up and down edges

(c) variation of τ_{yx} at left and right edges

(d) variation of τ_{xy} at up and down edges

Fig.5
Variation of in-plane stress components for uniaxial loading at plate edges for $D/a = 0.6$.

Fig. 6 shows the contour plot of the pre-buckling stress components for $D/a = 0.6$, which are calculated based on the presented solution.

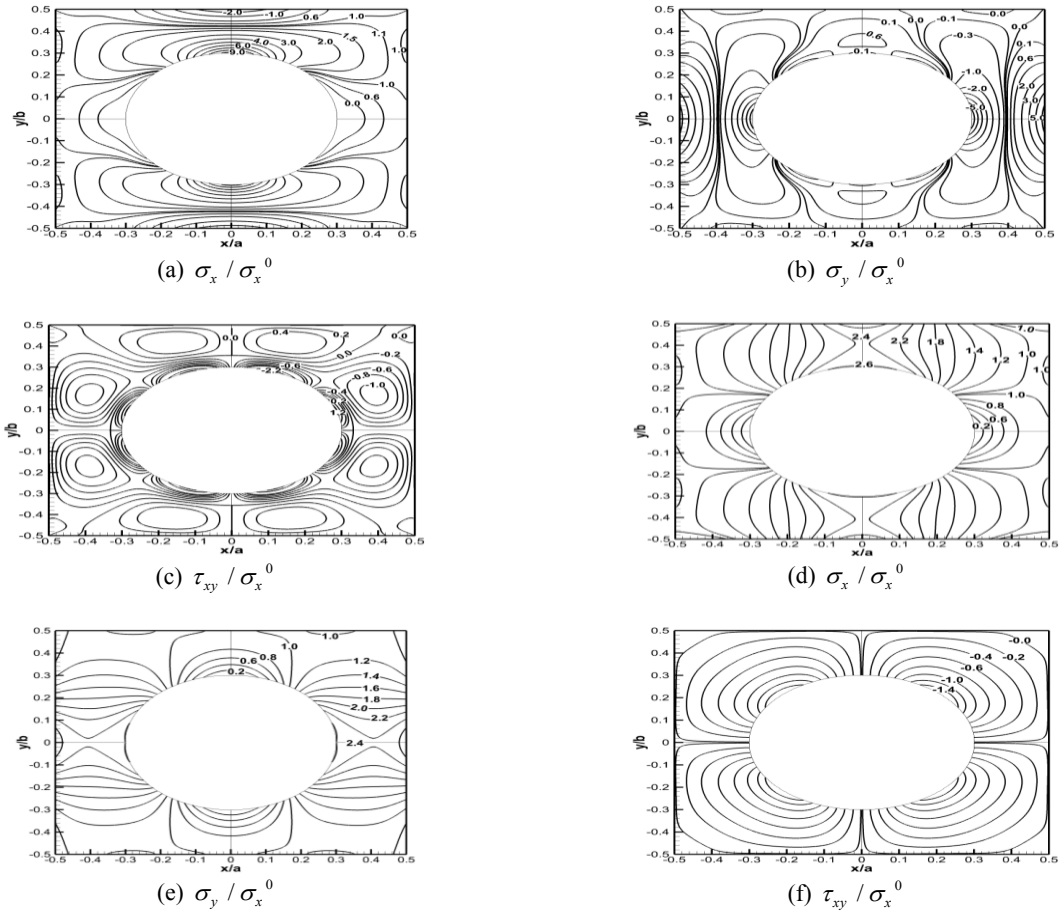

(a) $\sigma_x / \sigma_x{}^0$

(b) $\sigma_y / \sigma_x{}^0$

(c) $\tau_{xy} / \sigma_x{}^0$

(d) $\sigma_x / \sigma_x{}^0$

(e) $\sigma_y / \sigma_x{}^0$

(f) $\tau_{xy} / \sigma_x{}^0$

Fig.6
Contour plot of pre-buckling stress components, a-c) uniaxial loading, d-e) biaxial loading.

4.2 Buckling

In order to calculate the plate buckling load, the pre-buckling stress components are substituted in Eq. (15) and the Gauss quadrature method is used for integration. Then, based on the Ritz minimization method, an eigenvalue problem has been constructed to find the buckling load. The values of *M=N=9* have been selected in Eq. (19), for convergence. Comparison of the buckling load obtained by the present analytical solution with the existing numerical results has been summarized in Table 1. for simply supported and clamped plates. The buckling load is normalized as $\bar{N}_{cr} = N_{cr} b^2 / \pi^2 D_{11}$ where $D_{11} = Eh^3 / 12(1-\nu^2)$ is the flexural rigidity of the plate. The maximum difference is about 6% for SSSS boundary condition for both uniaxial and biaxial loading, while for CCCC plate the maximum difference is 13% for uniaxial loading and 7% for biaxial loading.

Table 1
Comparison of normalized buckling load $\bar{N}_{cr}$ with existing results.

	Uniaxial						Biaxial			
	SSSS				CCCC		SSSS		CCCC	
D/a	Present	Sabir and Chow [13]	El-Sawy and Nazmy [12]	Komur and Sonmez [20]	Present	Sabir and Chow [13]	Present	Sabir and Chow [13]	Present	Sabir and Chow [13]
0	3.986	------	4.000	4.002	9.914	------	1.993	------	5.234	------
0.1	3.924	3.691	3.859	3.861	9.723	9.530	1.962	1.849	5.207	4.843
0.2	3.571	3.445	3.531	3.527	8.958	------	1.794	1.766	5.019	4.714
0.3	3.230	3.185	3.240	3.230	8.735	8.534	1.640	1.640	5.307	5.086
0.4	3.023	3.049	3.040	3.037	8.381	8.728	1.568	1.545	6.128	5.986
0.5	2.890	2.840	2.914	2.906	7.801	9.005	1.554	1.473	7.215	7.514
0.6	2.818	------	2.829	2.817	7.099	------	1.586	------	8.529	------

The effect of different combinations of boundary conditions and D/a ratio on the buckling load of a square plate with circular cutout has been presented in Tables 2 and 3 for uniaxial and biaxial loadings, respectively. The results have been compared with the FE solutions, which show the good agreement. In these Tables, each type of boundary condition has been named by a four-letter word, where the first two letters represent the boundary conditions in *x* direction and the other letters represent the boundary condition in *y* direction. Also *S, C* and *F* stand for simply supported, clamped and free boundary conditions, respectively. According to Tables 2 and 3, increasing the size of the cutout decreases the buckling load for all types of boundary conditions for uniaxial loading. But for biaxial loading, the *CCCC* case has a different behavior in which the buckling load increases for higher D/a ratios. The value of buckling load depends on the plate supports and the plates with *CCCC* and *SSFF* boundary conditions have the highest and lowest buckling loads, respectively. Note that the reduction in buckling load for $D/a = 0.6$ relative to a plate without hole for uniaxial loading is equal to 28.39% for *CCCC* and 54.01% for *SSFF* case. For the plates subjected to biaxial loading, this reduction is 20.41 % for *SSSS* and 62.95% for *CCCC* plate. For the other types of boundary conditions, this reduction is between these two values. The buckling load of the plates under biaxial loading is lower than the plates with uniaxial loading. The plates with *SSFF* boundary condition have similar behavior under uniaxial and biaxial loading.

Figs. 7 and 8 show the sensitivity of the buckling load to pre-buckling stress field. In these Figures, the buckling load has been calculated by assuming a constant pre-buckling stress field, i.e $\sigma_x = \sigma_x^0, \sigma_y = 0, \tau_{xy} = 0$ for uniaxial loading and $\sigma_x = \sigma_x^0, \sigma_y = \sigma_x{}^0, \tau_{xy} = 0$ for biaxial loading, and this value is compared with the buckling load from the obtained results from the pre-buckling stress field. According to Figs. 7 and 8, the sensitivity of the buckling load to pre-buckling stress field depends on the boundary conditions and D/a ratio. For uniaxial loading, the buckling load of a plate with *SSFF* boundary condition has the lowest sensitivity with the maximum difference equal to 10.67%, while the buckling load of a plate with *CCFF* boundary condition is very sensitive to pre-buckling stress distribution and the maximum difference in this case is 63.89%. For biaxial loading, the plates with *SSFF* and *CCSF* boundary conditions have the lowest and highest sensitivity to pre-buckling stresses and the maximum difference for

these two cases is 12.81% and 40.24%, respectively. When D/a ratio increases, the non-uniformity in the pre-buckling stress field increases and as a result, the sensitivity of the buckling load to pre-buckling stress field increases. The effect of plate thickness on the buckling load for uniaxial loading has been presented in Table 4. In this Table, the buckling load for *CPT* has been compared with the *FSDT* and *FE* results. For *CPT*, the rotations u_1, v_1 are equal to $-\partial w_0/\partial x$ and $-\partial w_0/\partial y$, respectively and the traverse shear stresses are zero, while in *FSDT*, these stress components are constant along the plate thickness. The normalized buckling load $\bar{N}_{cr}$ from *CPT* is independent of the thickness ratio (*a/h*), which means that the buckling load is proportional to h^3 (because $\bar{N}_{cr} = N_{cr} b^2/\pi^2 D_{11}$ and D_{11} is proportional to h^3). The accuracy of *CPT* in estimating the buckling load decreases as the plate thickens. The difference between calculated buckling load from *CPT* and *FSDT* depends strongly on the plate boundary conditions where, for *CCCC* plate, the maximum difference is 73.55% and for *SSFF*, the maximum difference is 4%.

Table 2
Normalized Buckling load ($\bar{N}_{cr}$) of a square plate with circular cutout under uniaxial loading.

D/a	Boundary Conditions											
	SSSS		CCCC		SSFF		CCFF		SSSF		CCSF	
	Present	FE	Present	FE	Present	FE	Present	FE	Present	FE	Present	FE
0	3.986	3.989	9.914	9.964	0.960	0.950	3.911	3.896	1.417	1.395	4.373	4.340
0.1	3.924	3.833	9.723	9.375	0.942	0.921	3.845	3.785	1.403	1.364	4.320	4.225
0.2	3.571	3.508	8.958	8.682	0.865	0.846	3.607	3.547	1.334	1.280	4.108	3.969
0.3	3.230	3.220	8.735	8.458	0.759	0.747	3.347	3.289	1.213	1.165	3.790	3.670
0.4	3.023	3.019	8.381	8.286	0.649	0.640	3.085	3.009	1.065	1.034	3.459	3.299
0.5	2.890	2.885	7.801	7.866	0.543	0.533	2.732	2.653	0.912	0.889	3.031	2.811
0.6	2.818	2.782	7.099	7.176	0.442	0.428	2.287	2.199	0.754	0.729	2.464	2.248

Table 3
Normalized Buckling load ($\bar{N}_{cr}$) of a square plate with circular cutout under biaxial loading.

D/a	Boundary Conditions											
	SSSS		CCCC		SSFF		CCFF		SSSF		CCSF	
	Present	FE	Present	FE	Present	FE	Present	FE	Present	FE	Present	FE
0	1.993	1.994	5.234	5.258	0.941	0.929	2.755	2.687	1.077	1.047	2.864	2.803
0.1	1.962	1.918	5.207	5.023	0.923	0.903	2.777	2.671	1.067	1.030	2.874	2.765
0.2	1.794	1.764	5.019	4.863	0.853	0.833	2.718	2.616	1.030	0.983	2.797	2.669
0.3	1.640	1.638	5.307	5.213	0.753	0.740	2.603	2.506	0.965	0.913	2.653	2.535
0.4	1.568	1.569	6.128	6.177	0.648	0.637	2.420	2.330	0.874	0.828	2.441	2.344
0.5	1.554	1.556	7.215	7.801	0.544	0.533	2.169	2.084	0.766	0.729	2.172	2.089
0.6	1.586	1.587	8.529	8.084	0.440	0.431	1.867	1.787	0.644	0.617	1.859	1.787

Table 4
Normalized buckling load ($\bar{N}_{cr}$) of a plate under uniaxial loading from different methods.

Boundary Condition	*D/a*	CPT	*a/h*=40		*a/h*=20		*a/h*=10	
			FSDT	FE	FSDT	FE	FSDT	FE
CCCC	0	10.037	9.914	9.964	9.561	9.582	8.358	8.310
	0.1	9.843	9.723	9.375	9.381	9.027	8.210	7.863
	0.2	9.070	8.958	8.682	8.638	8.349	7.537	7.231
	0.3	8.889	8.735	8.458	8.318	8.044	6.978	6.721
	0.4	8.600	8.381	8.286	7.812	7.694	6.153	6.018
	0.5	8.097	7.801	7.866	7.083	7.080	5.239	5.145
	0.6	7.454	7.099	7.176	6.258	6.231	4.295	4.145
SSFF	0	0.943	0.960	0.929	0.935	0.944	0.912	0.923
	0.1	0.925	0.942	0.903	0.917	0.914	0.895	0.893
	0.2	0.855	0.865	0.833	0.847	0.840	0.825	0.819
	0.3	0.755	0.759	0.740	0.747	0.741	0.728	0.724
	0.4	0.650	0.649	0.637	0.643	0.635	0.627	0.621
	0.5	0.546	0.543	0.533	0.539	0.529	0.526	0.519
	0.6	0.442	0.442	0.431	0.436	0.425	0.425	0.418

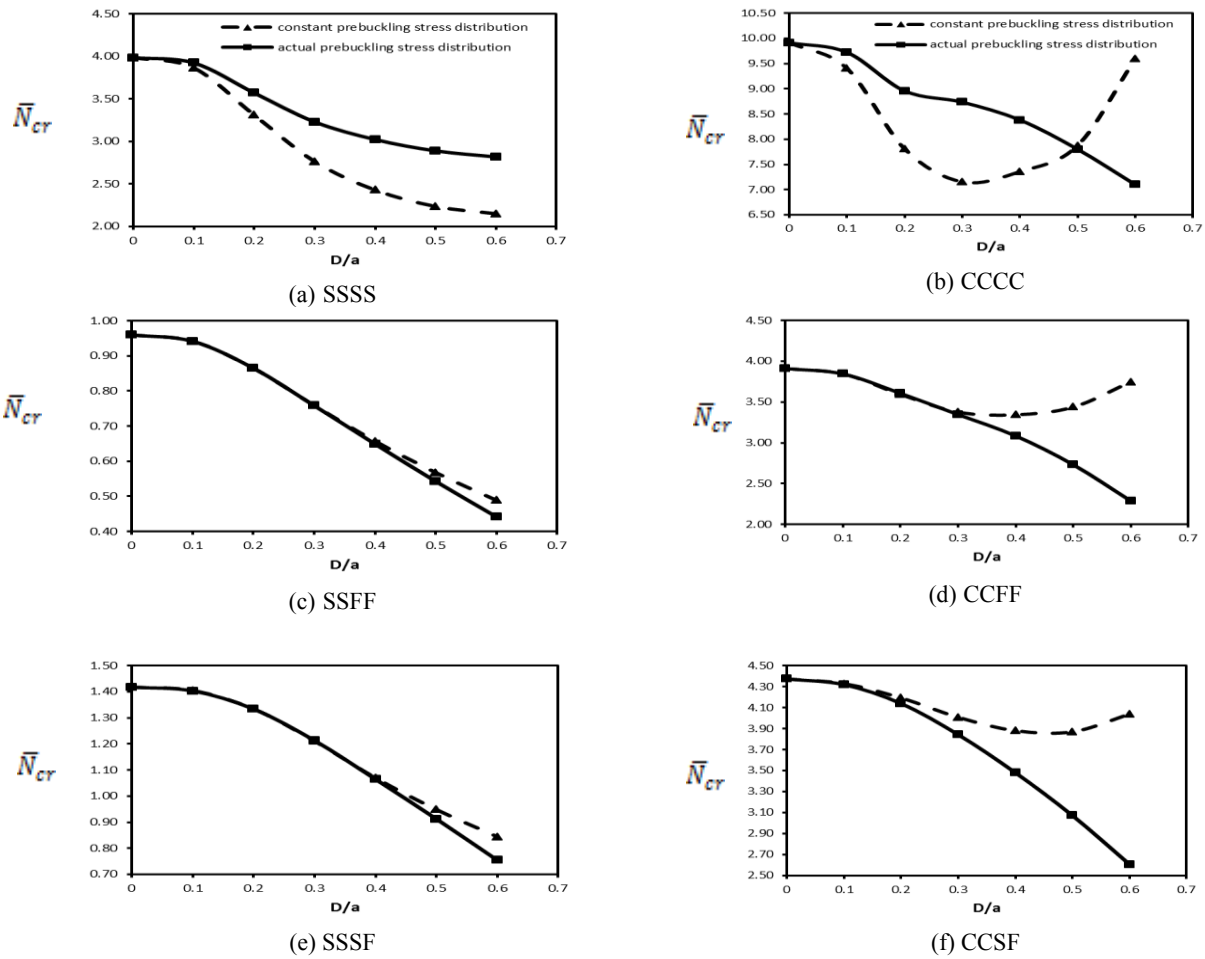

(a) SSSS (b) CCCC

(c) SSFF (d) CCFF

(e) SSSF (f) CCSF

Fig.7
Sensitivity of buckling load to pre-buckling stress field for uniaxial loading.

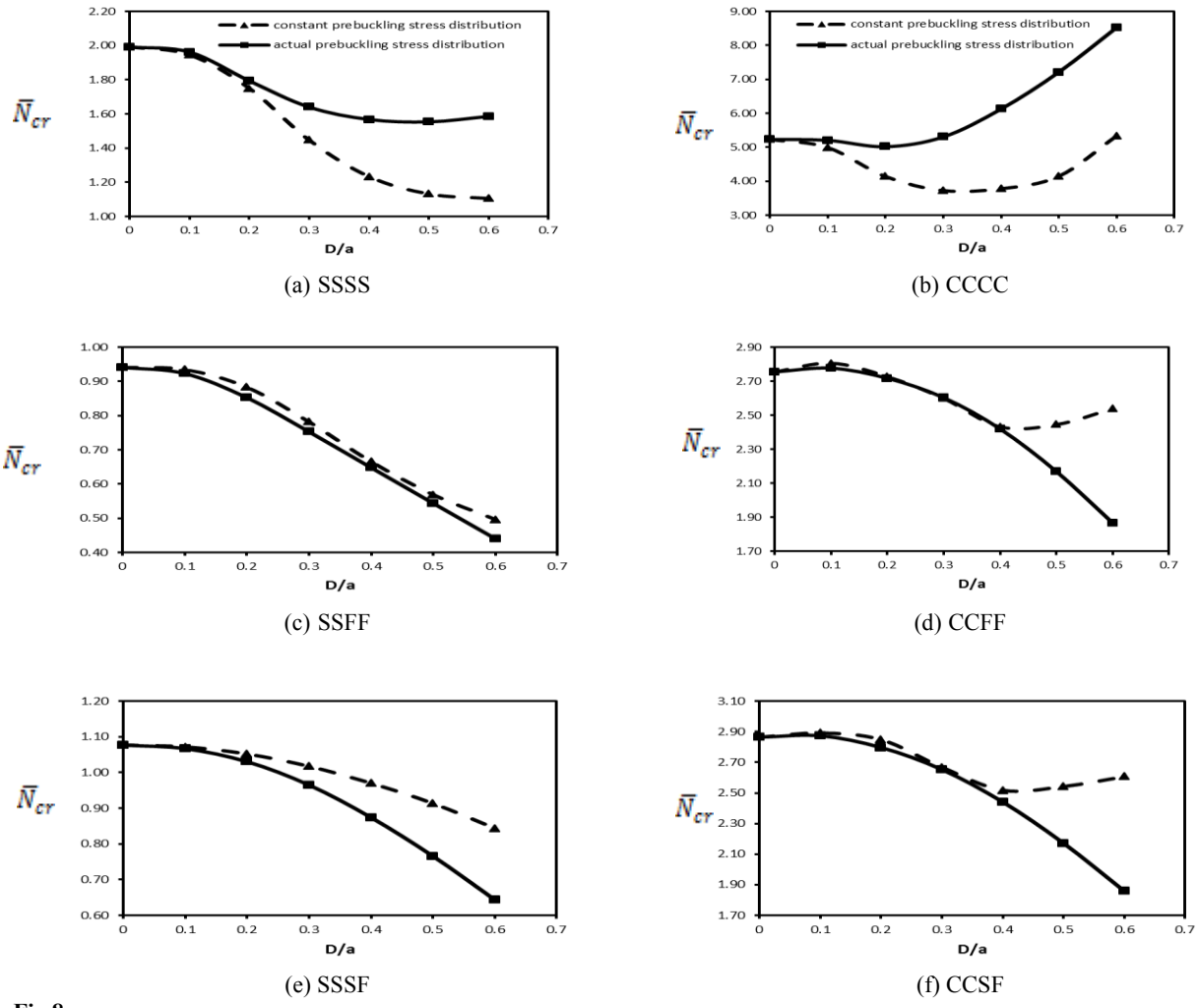

(a) SSSS (b) CCCC

(c) SSFF (d) CCFF

(e) SSSF (f) CCSF

Fig.8

Sensitivity of buckling load to pre-buckling stress field for biaxial loading.

5 CONCLUSIONS

Buckling of the plates with circular cutout under in-plane uniaxial and biaxial loading was investigated in this study. The presence of cutout alters the stress distribution in the plate compared with a plate without cutout. In order to calculate the buckling load, this stress distribution must be known. The complex potential method was used in conjunction with the boundary integral based on the principle of virtual work to obtain the pre-buckling stress distribution. The buckling load was calculated by using the vibrational mode shapes of a Euler-Bernoulli beam to represent the displacement components in the Ritz method. The effect of different combinations of boundary conditions, loading type and D/a ratio on the buckling load was analyzed. The results can be summarized as follows:

- When the D/a ratio increases, the plate buckles in lower loads for all boundary conditions.
- The buckling loads of plates with *CCCC* and *SSFF* boundary conditions have the highest and lowest values, respectively, in both uniaxial and biaxial loading.
- The buckling load of the plates under biaxial loading is lower than the plates with uniaxial loading.
- The sensitivity of the buckling load to pre-buckling stress distribution depends on the boundary conditions and D/a ratio.

- For uniaxial loaded plates, the buckling load of *SSFF* plates has the lowest sensitivity to the pre-buckling stress while the buckling load of *CCFF* plates is very sensitive to pre-buckling stress.
- For biaxial loaded plates, the plates with *SSFF* and *CCSF* boundary conditions have the lowest and highest sensitivity to the pre-buckling stresses.
- By increasing D/a ratio, the sensitivity of the buckling load to pre-buckling stress distribution increases.
- The difference between *CPT* and *FSDT* in calculating the buckling load depends on the plate boundary conditions and the accuracy of *CPT* decreases as the plate thickness increases.

REFERENCES

[1] Lekhnitskii S., 1968, *Anisotropic Plates*, Gordon and Breach Science, New York.

[2] Savin G. N., *1961,Stress Concentration Around Holes*, Pergamon, New York.

[3] Sevenois R. D. B., Koussios S., 2014, Analytic methods for stress analysis of two-dimensional flat anisotropic plates with notches: an overview, *Applied Mechanics Reviews* **66**: 060802.

[4] Lin C. C., Ko C. C., 1988, Stress and strength analysis of finite composite laminates with elliptical holes, *Journal of Composite Materials* **22**: 373-385.

[5] Gao X. L., 1996, A general solution of an infinite elastic plate with an elliptic hole under biaxial loading, *International Journal of Pressure Vessels and Piping* **67**: 95-104.

[6] Ukadgaonker V. G., Rao D. K. N., 2000, A general solution for stresses around holes in symmetric laminates under inplane loading, *Composite Structures* **49**: 339-354.

[7] Xu X. W., Man H. C., Yue T. M., 2000, Strength prediction of composite laminates with multiple elliptical holes, *International Journal of Solids and Structures* **37**: 2887-2900.

[8] Louhghalam A., Igusa T., Park C., Choi S., Kim K., 2011, Analysis of stress concentrations in plates with rectangular openings by a combined conformal mapping – Finite element approach, *International Journal of Solids and Structures* **48**: 1991-2004.

[9] Nemeth M. P., stein M., Johnson E. R., 1986, An approximate buckling analysis for rectangular orthotropic plates with centrally located cutouts, *NASA Technical Paper* **1986**: 1-18.

[10] Britt V. O., 1994, Shear and compression buckling analysis for anisotropic panels with elliptical cutouts, *AIAA Journal* **32**: 2293-2299.

[11] Shakerley T. M., Brown C. J., 1996, Elastic buckling of plates with eccentrically positioned rectangular perforations, *International Journal of Mechanical Sciences* **38**: 825-838.

[12] El-Sawy K. M., Nazmy A. S., 2001, Effect of aspect ratio on the elastic buckling of uniaxially loaded plates with eccentric holes, *Thin–Walled Structures* **39**: 983-998.

[13] Sabir A., Chow F., 1986, Elastic buckling of plates containing eccentrically located circular holes, *Thin–Walled Structures* **4:** 135-149.

[14] Ghannadpour S. A. M., Najafi A., Mohammadi B., 2006, On the buckling behavior of cross-ply laminated composite plates due to circular/elliptical cutouts, *Composite Structures* **75**: 3-6.

[15] Anil V., Upadhyay C. S., Iyengar N. G. R., 2007, Stability analysis of composite laminate with and without rectangular cutout under biaxial loading, *Composite Structures* **80**: 92-104.

[16] Moen C. D., Schafer B. W., 2009, Elastic buckling of thin plates with holes in compression or bending, *Thin–Walled Structures* **47**: 1597-1607.

[17] Kumar D., Singh S. B., 2013, Effects of flexural boundary conditions on failure and stability of composite laminate with cutouts under combined in-plane loads, *Composites Part B: Engineering* **45**: 657-665.

[18] Kumar D., Singh S. B., 2012, Stability and failure of composite laminates with various shaped cutouts under combined in-plane loads, *Composites Part B: Engineering* **43**: 142-149.

[19] Kumar D., Singh S. B., 2010, Effects of boundary conditions on buckling and postbuckling responses of composite laminate with various shaped cutouts, *Composite Structures* **92**: 769-779.

[20] Aydin Komur M., Sonmez M., 2008, Elastic buckling of rectangular plates under linearly varying in-plane normal load with a circular cutout, *Mechanics Research Communications* **35**: 361-371.

[21] Prajapat K., Ray-Chaudhuri S., Kumar A., 2015, Effect of in-plane boundary conditions on elastic buckling behavior of solid and perforated plates, *Thin–Walled Structures* **90**: 171-181.

[22] Barut A., Madenci E., 2010, A complex potential-variational formulation for thermo-mechanical buckling analysis of flat laminates with an elliptic cutout, *Composite Structures* **92**: 2871-2884.

[23] Ovesy H. R., Fazilati J., 2012, Buckling and free vibration finite strip analysis of composite plates with cutout based on two different modeling approaches, *Composite Structures* **94**: 1250-1258.

[24] Huang C., Leissa A., 2009, Vibration analysis of rectangular plates with side cracks via the Ritz method, *Journal of Sound and Vibration* **323**: 974-988.

[25] Huang C., Leissa A., Chan C., 2011, Vibrations of rectangular plates with internal cracks or slits, *International Journal of Mechanical Sciences* **53**: 436-445.

[26] Sadd M. H., 2005, *Elasticity: Theory, Applications, and Numerics*, Academic Press, India.
[27] Reddy J. N., 2006, *Theory and Analysis of Elastic Plates and Shells*, CRC Press.
[28] Bažant Z. P., Cedolin L., 2010, *Stability of Structures: Elastic, Inelastic, Fracture and Damage Theories*, World Scientific.
[29] Kumar Y., 2017, The Rayleigh–Ritz method for linear dynamic, static and buckling behavior of beams, shells and plates: A literature review, *Journal of Vibration and Control* **2017**: 1-23.
[30] Moreno-García P., Dos Santos J. V. A., Lopes H., 2017, A review and study on Ritz Method admissible functions with emphasis on buckling and free vibration of isotropic and anisotropic beams and plates, *Archives of Computational Methods in Engineering* **2017**: 1-31.
[31] ABAQUS, 6.11. User's manual, Dassault Systemes, 2011.